

Supporting information for:

Background reduction in STED-FCS using a bi-vortex phase mask

Aurélien Barbotin¹, Iztok Urbančič^{2,3,*}, Silvia Galiani^{2,4}, Christian Eggeling^{2,4,5,6,*} and Martin Booth¹

1 Department of Engineering Science, University of Oxford, Parks Road, Oxford OX1 3PJ, UK

2 MRC Human Immunology Unit, MRC Weatherall Institute of Molecular Medicine, University of Oxford, Oxford OX3 9DS, UK

3 "Jožef Stefan" Institute, Jamova cesta 39, SI-1000 Ljubljana, Slovenia

4 Wolfson Imaging Centre Oxford, MRC Weatherall Institute of Molecular Medicine, University of Oxford, Oxford OX3 9DS

5 Institute of Applied Optics and Biophysics, Friedrich-Schiller-University Jena, Max-Wien Platz 4, 07743 Jena, Germany

6 Leibniz Institute of Photonic Technology e.V., Albert-Einstein-Strasse 9, 07745 Jena, Germany

[*iztok.urbancic@ijs.si](mailto:iztok.urbancic@ijs.si), christian.eggeling@rdm.ox.ac.uk

10 pages; 7 figures; 1 table

Data fitting

We designed the fitting methods as described in reference¹. Because conventional fluorophores do not have a high enough molecular brightness to fit at the same time axial and lateral transit times, we instead fitted the observation volume with a prescribed shape. The exact shape of the observation volume depends on the STED confinement mode and was determined from pictures of immobilised 40 nm crimson beads.

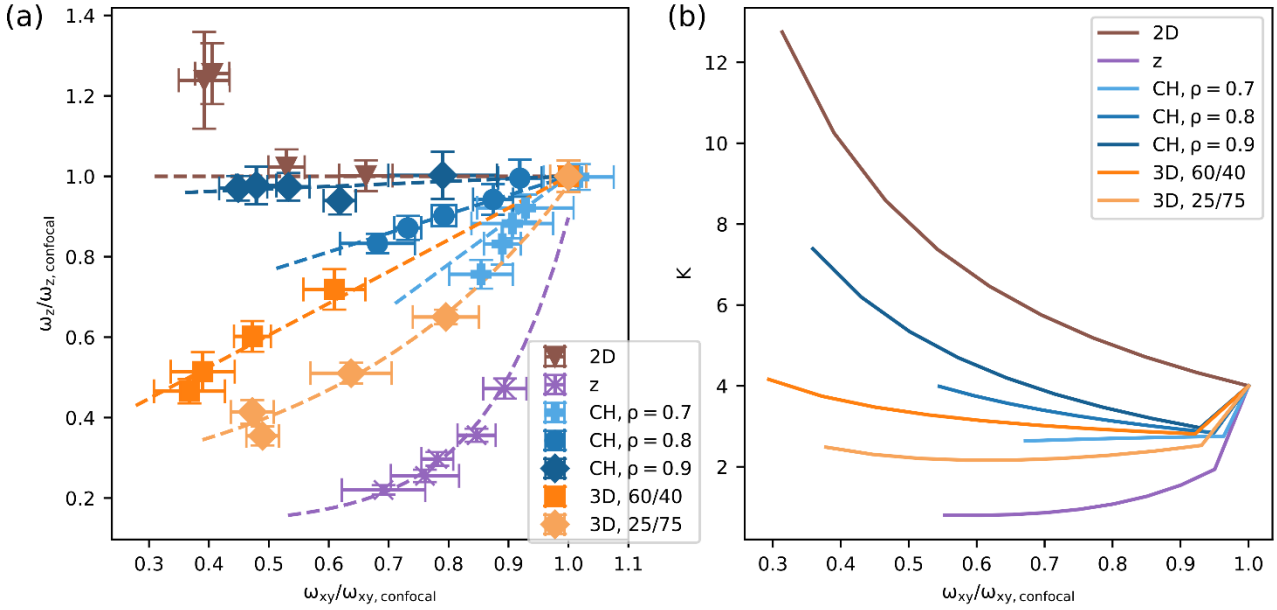


Figure S1: Experimental determination of the aspect ratio of the observation volume as a function of its lateral size for different STED confinement modes. (a) Measurement of resolution variations with STED laser power using fluorescent beads for different STED confinement modes, presented as two-dimensional plot of value pairs of lateral ω_{xy} and axial ω_z $1/e^2$ radius, normalised with confocal values (mean \pm std, $n = 10$ beads per datapoint). For 3D-STED, the fraction of energy going in each arm (2D/z) is specified in the legend. (b) Aspect ratio K as a function of lateral ω_{xy} $1/e^2$ radius normalised with its confocal value, determined from the fits to the data in panel (a) and used to fit STED-FCS data.

For each STED confinement mode and at STED laser powers ranging from 0 (confocal) to 150 mW, we acquired a set of three-dimensional image stacks of fluorescent beads. In each of the stacks, 7 to 10 beads were manually selected, and their axial cross-section was fitted with a two-dimensional Gaussian ellipsoid to estimate their lateral and axial full width at half maximum. Results are presented in Figure S1a. The variation of axial resolution with lateral resolution was then fitted with either an exponential or a linear function, allowing description of the shape of the observation volume with a single parameter (τ_{xy} , with $K = K(\tau_{xy}/\tau_{xy, \text{confocal}})$ being pre-calibrated) instead of two (τ_{xy} and K). The calibrated values of K as a function of the lateral size of the observation volume are presented in Figure S1b. To account for the remaining system aberrations and spherical aberrations, which elongate the observation volume in FCS but not when imaging fluorescent beads, as outlined in Figure 2 in the main text and in Figure S2, we set the confocal aspect ratio to 4 in confocal FCS, larger than the value of 2.8 measured in imaging. This correction accounted for both the observed

elongation and deformation (from Gaussian to Lorentzian). With all STED confinement modes except for 2D STED, we assumed that these contributions along the optical axis were efficiently depleted by the aberration-corrected STED laser even at low STED laser power, thus recovering the observation volume shapes measured in imaging. This led to in practice higher aspect ratios in 2D-STED than in other confinement modes, even at moderate STED laser powers. We used these different models throughout the paper, with the exception of Figure 4 in the main text, where we preferred using a consistent model to analyse all data points instead of the physically more accurate discontinuous model we used in the rest of the paper.

Fitting two-dimensional Gaussian functions to axial images of fluorescent beads with 2D-STED, we found an increase in axial size (Figure S1a, brown triangles), most likely caused by a more efficient depletion of fluorescence in the focal plane, leading to an off-focus broadening and as such an increased axial dimension. This effect was previously described², and is in part responsible for the poor performance of 2D-STED-FCS in three dimensions.

Shape of confocal and STED observation volumes estimated from images of fluorescent beads

We verified using images of fluorescent beads that the shape of the STED and confocal observation volumes could be well approximated with a Gaussian function. To do this, we used the axial profiles of fluorescent beads described in the previous section. For each STED confinement mode and each STED laser power, we fitted a two-dimensional Gaussian, Lorentzian, or Gaussian-Lorentzian function to the axial images of fluorescent beads. To estimate which function fitted the data best, we compared the residuals of each fit to the residuals obtained with a Gaussian fit. In most cases, the Gaussian fit provided the smallest residuals, suggesting that the observation volume was indeed Gaussian. Only 2D-STED at the highest STED laser power was better described by a Gaussian profile along z and Lorentzian profile along x , with an extremely small difference. Overall, our results confirmed that the different volumes used throughout this study were well described by a Gaussian function.

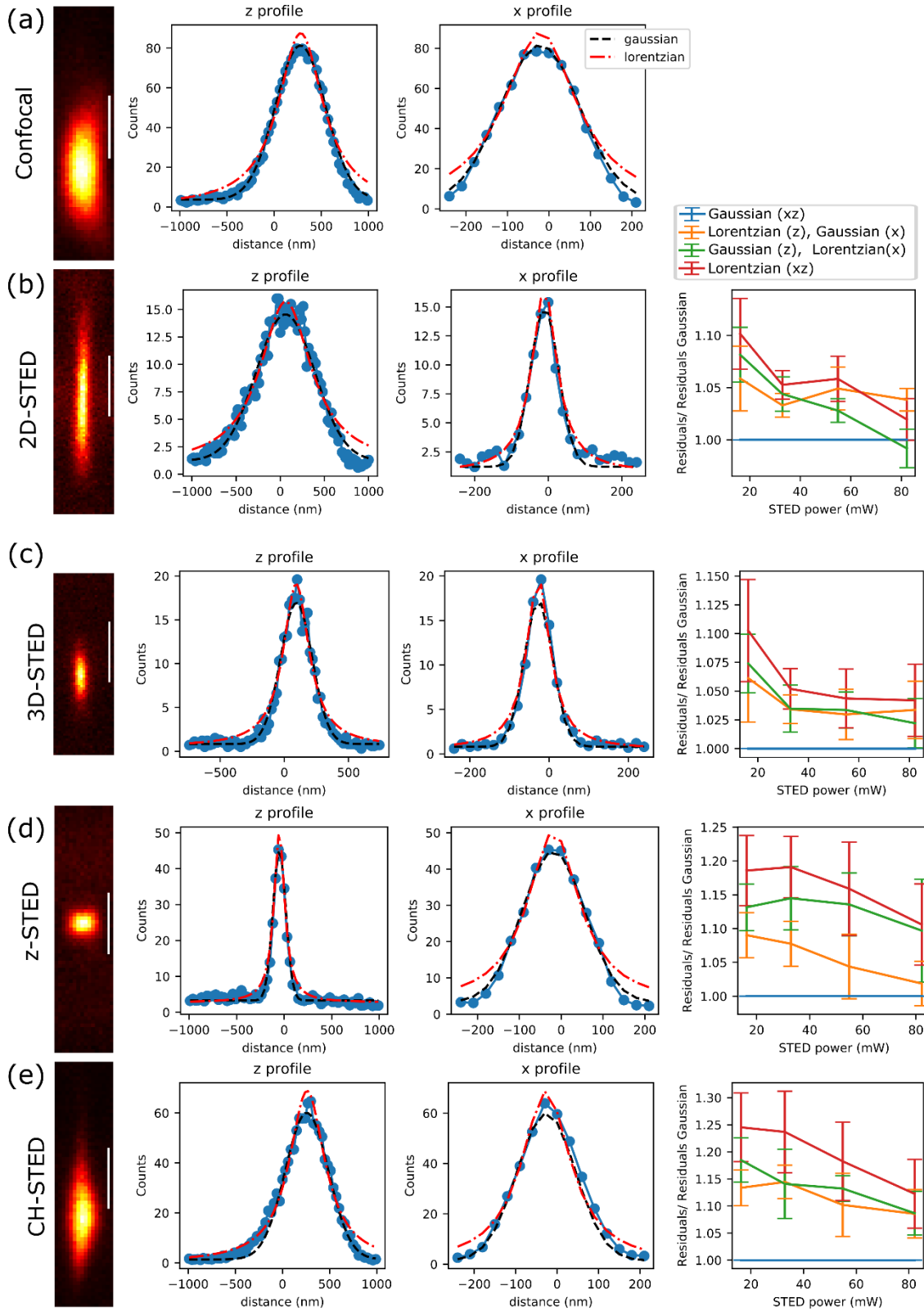


Figure S2: Estimating the shape of STED observation volumes by imaging fluorescent beads. (a-e) left: Average of 10 axial images of fluorescent beads imaged in confocal (a), 2D-STED (b), 3D-STED (c), z-STED (d) and CH-STED (e), and axial (middle left) and lateral (middle right) profiles fitted with a Gaussian (black) or Lorentzian (red) function. Scale bars: 500 nm. (b-e), right: fitting residuals obtained with a Gaussian, Lorentzian, or Gaussian-Lorentzian function as indicated in the legend; Error bars: standard deviation, $n = 10$ measurements.

Estimation of signal-to-background ratio in simulated data

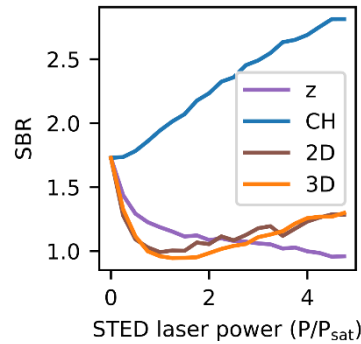


Figure S3: Simulation of signal-to-background ratio (SBR), integrated across all three dimensions varying with STED laser power (normalised to the saturation power P_{sat}) for different STED confinement modes as indicated in the legend

In order to quantify differences between STED confinement modes in simulations, we integrated the spatial contributions of signal and background. STED laser powers were normalised with a saturation power P_{sat} defined as the STED laser power leading to a 2-fold lateral resolution improvement in 2D STED. Background was defined as low-intensity contributions, below a threshold equal to $1/e^2$ of the maximum intensity². SBR measured with this method suggested that CH-STED depletes background most effectively. However, several inconsistencies with experimental data appeared at high simulated STED laser powers, with 2D and 3D STED increasing SBR instead of reducing it. Indeed, at high STED laser power, even small intensity contributions in areas of poor overlap between excitation and depletion foci get depleted. In a real experiment, imperfections in the depletion focus would lead to a drastic reduction in signal levels, largely overcoming this effect. Though it is convenient to model background as low intensity contributions below a certain threshold, it is most likely an imperfect model that does not describe the physical reality accurately. Indeed, with this model, even a perfect Gaussian excitation focus exhibits uncorrelated background contributions, which does not match experimental results. Finally, our model also omitted other physical effects such as STED re-excitation and residual scattered STED light measured by the detector.

FCS curves in solution

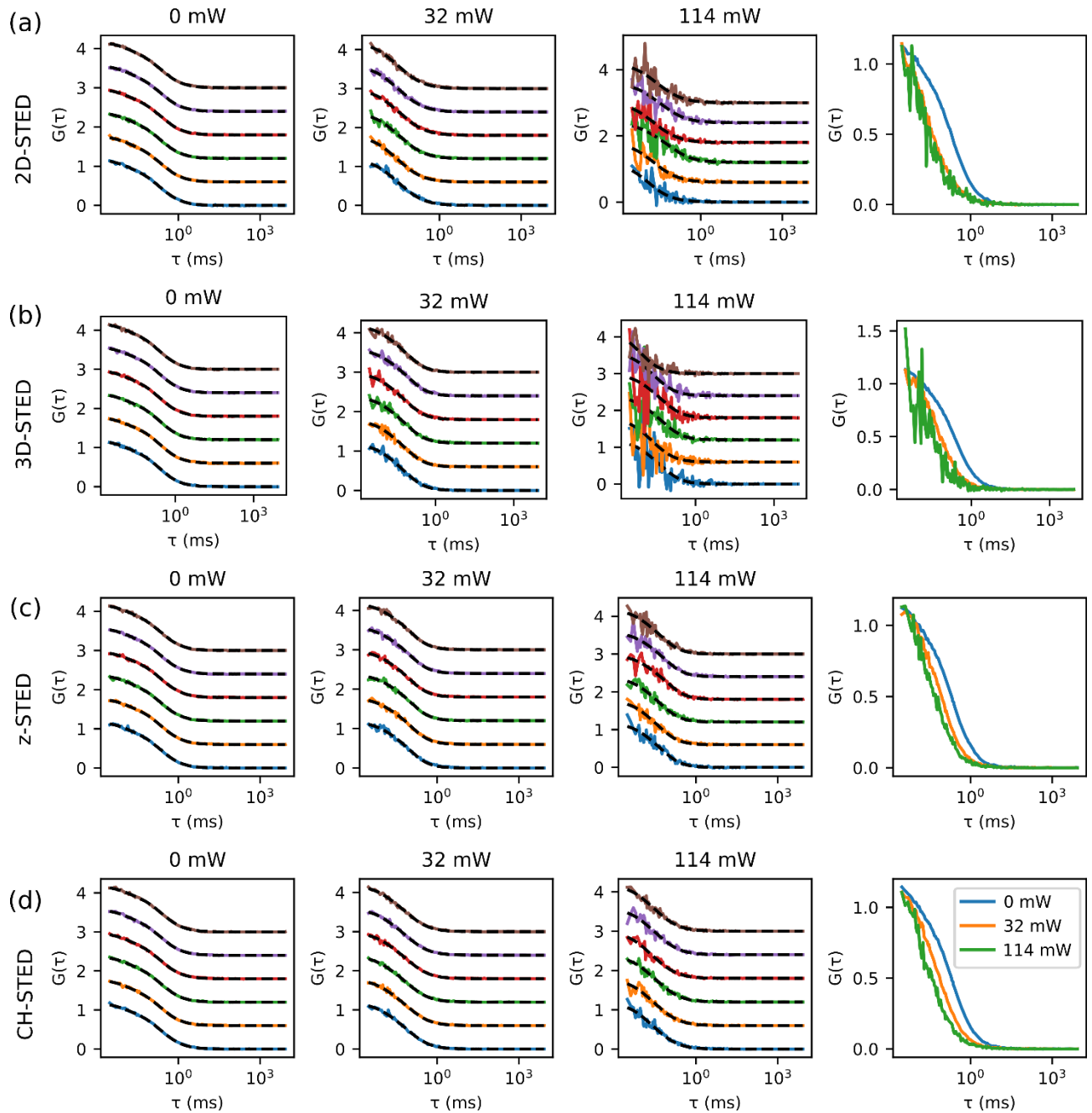


Figure S4: STED-FCS curves with different confinement modes in an aqueous solution of freely diffusing Abberior Star Red dyes. (a) 2D-STED, (b) 3D-STED, (c) z-STED and (d) CH-STED curves obtained at respectively 0 mW STED laser power (confocal, left), 32 mW (middle left) and 114 mW (middle right). Right: Median of normalised FCS curves at different STED laser power, as indicated in the legend in panel (d).

Aberrations

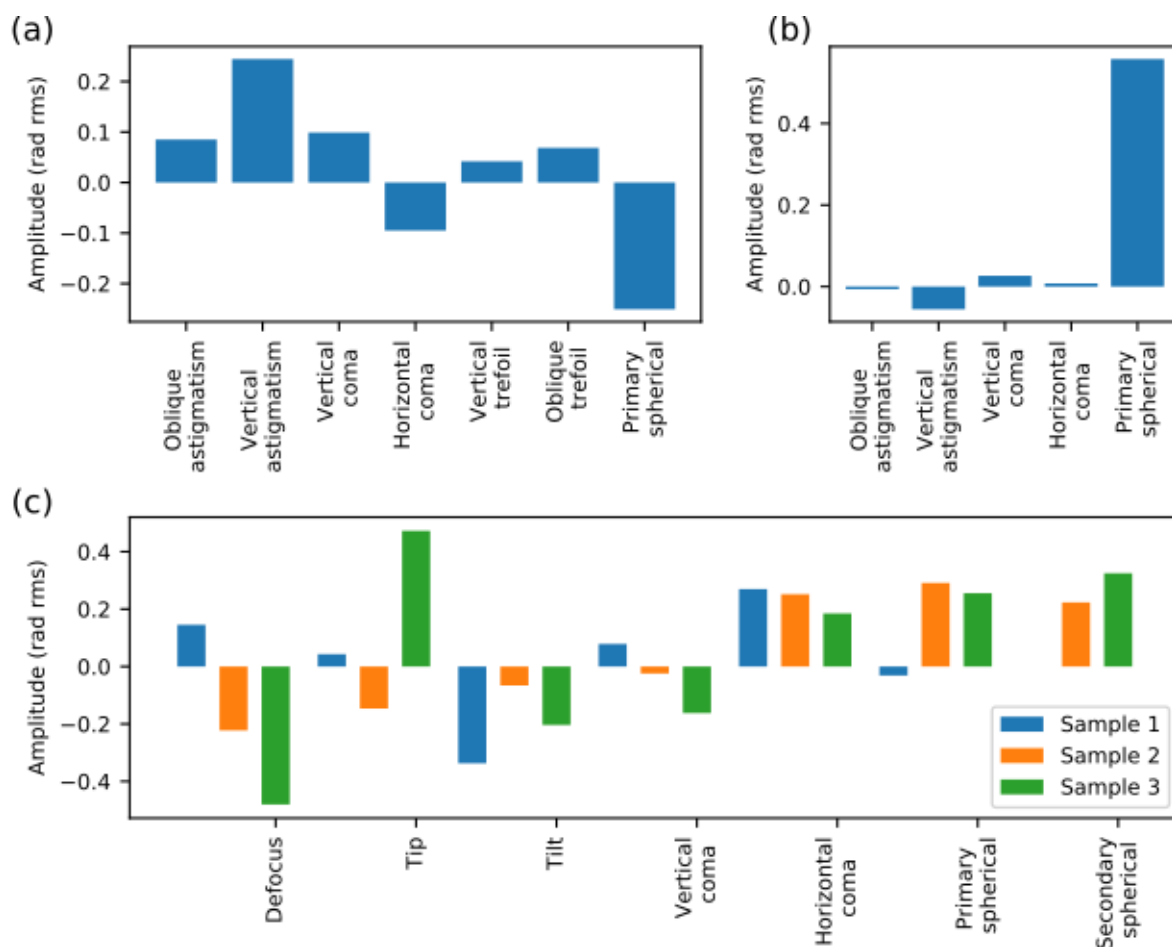


Figure S5: Aberration values measured experimentally. (a) System-induced aberrations, (b) typical aberration values found when measuring free diffusion in a solution of Abberior Star Red dyes in water:glycerol, and (c) aberrations measured in three cells samples, as indicated in the legend.

Aberrations in the depletion beam were corrected to ensure an optimal measurement quality. System-induced aberrations caused by misalignments or imperfections in the optical components were corrected first, using the sensorless method. A sample of scattering gold beads was scanned through the focus while various amounts of aberrations were induced by the SLM, and the image quality was assessed using the standard deviation of an image. The amplitude of system aberrations determined with this method was relatively low, limited to around 0.2 radians root mean square (rad rms) (Figure S5a). When measuring STED-FCS in a freely diffusing solution of Abberior Star Red dyes at penetration depths comprised between 3 and 5 μm , the refractive index mismatch between the immersion oil of the objective and the solution induced mostly spherical aberrations (Figure S5b), with an amplitude approximately equal to 0.5 rad rms. In cells, aberrations measured were more heterogeneous, with maximum amplitudes equal to 0.4 rad rms (Figure S5c). Misalignments

between excitation and depletion beam occurred because of the effect of thermal and mechanical drift, as we observed previously¹, and were corrected using tip, tilt and defocus.

Determination of triplet correlation parameters in solution

We determined triplet correlation times in a solution of Abberior Star Red dyes in a water:glycerol solution by fitting a series of confocal FCS curves recorded with an acquisition time of 60 s. Individual curves were fitted by equation (2) from main text, with an α factor set to 1 and an aspect ratio K set to 4. First, we visualised the effects of different triplet correlation times on the quality of fit (Figure S6a-b). Fixing the triplet correlation times to a relatively high value of 12 μ s yielded a better fit than a lower value of 5 μ s. We confirmed this by fitting a series of 17 confocal FCS curves, from which we could estimate the triplet correlation time τ_T (Figure S6c) and the triplet correlation amplitude T (Figure S6d). Results are summarised in Table S1.

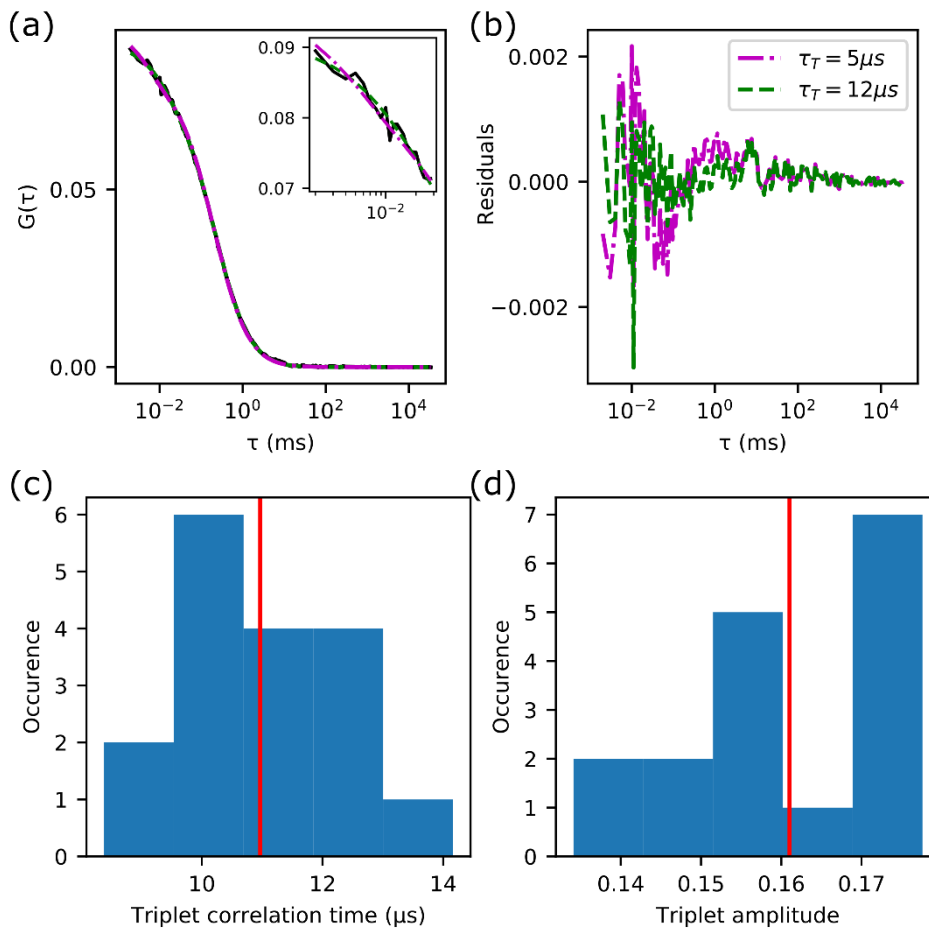


Figure S6: Determination of triplet parameters in a solution of Abberior Star Red dyes in a water:glycerol solution. (a) FCS curve obtained in solution with a long (60 s) acquisition time, fitted with different values of triplet correlation times fixed as indicated in the legend in panel (b). Inset: zoom on the short correlation times. (b) Residuals obtained when fitting the curve in (a) with either a triplet correlation time of 5 μ s (magenta) or 12 μ s (green). (c-d) Histograms of fit results for (c) triplet correlation time and (d) triplet correlation amplitude, with average value plotted in red. Histograms of 17 values, excitation power = 8 μ W.

Table S1: Triplet correlation parameters of Abberior Star Red in solution

Excitation power	τ_T	T
8 μ W	11 μ s	0.16
17 μ W	11 μ s	0.25

Determination of factor α in cells

Molecules diffusing in the cytoplasm do not diffuse freely but undergo subdiffusion due to the crowded molecular environment in the cytoplasm. In FCS, this is described with a parameter α (see equation (2) in main text). To determine the value of this parameter, we fitted a series of 45 confocal FCS curves acquired in cells and allowed variations of α . Curves were better fitted with values of α smaller than 1 (Figure S7a-b). We found that an average value of $\alpha=0.8$ best described diffusion in cells (Figure S7c).

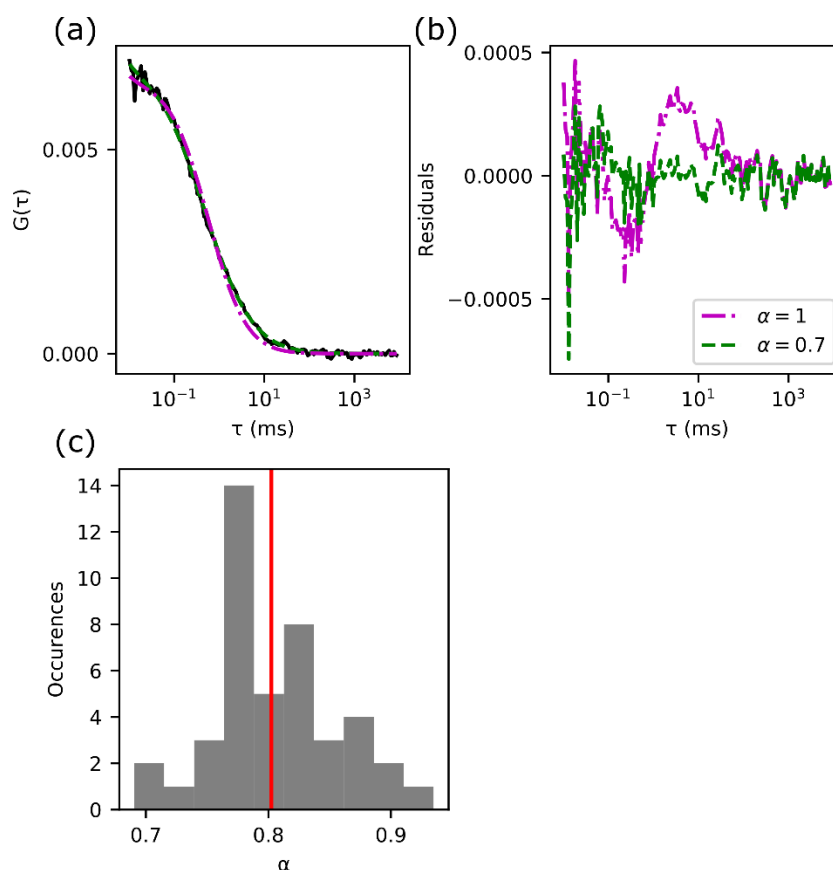


Figure S7: Determination of factor α in cells. (a) Representative confocal FCS curve obtained in a cell (black) and (b) the corresponding residuals of the curve fitted with different values of the factor α as described in the legend. (c) Histogram of parameters α obtained by fitting confocal FCS curves in cells, $n=45$ curves. Red line: average value.

References

- (1) Barbotin, A., Galiani, S., Urbančič, I., Eggeling, C. & Booth, M. J. Adaptive optics allows STED-FCS measurements in the cytoplasm of living cells. *Opt. Express* **27**, 23378–23395 (2019).
- (2) Sozanski, K., Sisamakos, E., Zhang, X. & Holyst, R. Quantitative fluorescence correlation spectroscopy in three-dimensional systems under stimulated emission depletion conditions. *Optica* **4**, 982–988 (2017).